Hydrogen Induced Cracking in HY-80 Steel Weldments

Direct observation of crack initiation and propagation, using an improved straining device, serves to clarify the role of hydrogen and the effect of rare earth additions

BY W. F. SAVAGE, E. F. NIPPES AND H. HOMMA

ABSTRACT. The development of a new testing procedure which reproduces hydrogen induced cracking in small laboratory scale specimens and allows direct observation of both initiation and propagation of the cracking is described. The testing device imposes an augmented strain on a transverse cross section of a bead-on-plate steel weldment. Results of cracking tests performed on four heats of HY-80 steel indicate that the device permits the quantitative evaluation of the susceptibility of different lots of the same material to hydrogen induced cracking.

Both the nucleation and propagation of hydrogen induced cracking were documented with both 35 mm still pictures and 16 mm motion pictures at magnifications of 100X or more. Evidence is presented indicating that a certain amount of microscopic yielding must occur locally before microcracks start to grow and that the presence of a sufficient amount of hydrogen is necesary for propagation of cracks to occur. The evidence supports the model which postulates that hydrogen makes localized deformation easier rather than causing embrittlement.

A documentation of the evolution of hydrogen bubbles from propagating cracks was made by putting a small amount of microscope immersion oil on the cracked surface. The results indicate that the planar-pressure mechanism would play no part in the propagation of hydrogen induced cracking.

It was found that hydrogen induced cracking was nucleated either by previously liquated grain boundaries and/or previously liquated nonmetallic inclusions in the unmixed zone and partially melted zone. It was also found that the cracking could be nucleated by elongated sulfide inclusions in the true heat-affected zone.

W. F. SAVAGE is Prof. of Metallurgical Engineering and Director of Welding Research, Renss. Poly. Inst., Troy, N.Y.; E. F. NIPPES is Prof. of Metallurgical Engineering, Renss. Poly. Inst.; H. HOMMA, formerly a Graduate Student at Renss. Poly. Inst., is now with the Products Research & Development Laboratories, Nippon Steel Corp., Sagamihara, Japan.

Introduction

In the welding of certain quenched and tempered, low alloy steels, a better understanding of the mechanisms involved in hydrogen induced cold cracking is required. The factors responsible for the problem have been summarized by other authors (Refs. 1-6). It is usually assumed that cold cracking is associated with hydrogen embrittlement of martensite or bainite and that it is initiated by high residual stresses developed in the weld joint during cooling.

At RPI, cold cracking in HY-80 weldments was found to be associated with both an unmixed zone of weld metal and a partially melted zone which exist between weld metal and true heat-affected zone (Refs. 7,8). Microcracks were nucleated at previously liquated grain boundaries and/or by previously liquated sulfide particles in these zones.

Cold cracking of HY-80 is reduced by the addition of rare earth elements (Ref. 9). This beneficial effect has been attributed to the fact that the globular rare earth sulfides have higher melting points than S compounds of other elements (e.g. Mn) and will not be liquated in the unmixed zone and/or partially melted zone.

Four basic mechanisms have been proposed to explain the observed results of hydrogen embrittlement (Ref. 10): (1) planar pressure, (Refs. 11,12), (2) adsorption on crack surfaces (Refs. 13,14,15), (3) reduction of binding energy (Ref. 16), and (4) modification of dislocation mobility (Refs. 17-22).

Indirect techniques (Refs. 23,24), rather than direct microscopic observation, have been used to study the fracture process of hydrogen induced cracking. A direct observation technique, initially proposed by Granjon (Ref. 25) and developed at RPI (Ref. 8), allows microscopic observation of initiation and propagation of cracks and of hydrogen bubble evolution from cracks in small externally stressed specimens. However, to date no study has been carried out under known applied stress or strain.

Objectives

The objectives of this investigation were:

1. To develop an improved testing device which reproduces hydrogen induced cracking in small laboratory scale samples and allows direct observation of both the initiation and propagation of the cracking.
2. To utilize this device to study the effect of the addition of rare earth elements and the magnitude of plastic deformation on hydrogen induced cracking in HY-80 weldments as a function of the amount of diffusible hydrogen present.

Table 1—Chemical Composition of HY-80 Used in This Investigation

Heat no.	Code no.	C	Mn	P	S	Si	Ni	Cr	Mo	Sol. Al	N	Rare earth (total)
66U438	Item 1	0.18	0.35	0.017	0.019	0.12	2.58	1.52	0.32	0.04	0.006	0.001
66U438	Item 2	0.17	0.33	0.018	0.015	0.13	2.55	1.54	0.31	0.04	0.007	0.029
66U438	Item 3	0.15	0.31	0.018	0.009	0.12	2.50	1.46	0.27	0.04	0.008	0.034
66U438	Item 4	0.17	0.32	0.016	0.008	0.11	2.50	1.45	0.27	0.04	0.007	0.11
72P305	Heat P	0.18	0.30	0.018	0.013	0.20	2.99	1.68	0.41	0.022	0.007	—

Experimental Procedure

Testing Devices

The testing devices shown schematically in Fig. 1 were designed, constructed and calibrated to facilitate the study of hydrogen induced cracking. In the first modification, which incorporated a four point bending load as shown in Fig. 1 (left) a constant elastic stress is produced on the outer fibers of the specimen between the two inner loading points.

Preliminary work, as will be discussed later, indicated that no macroscopic cracking resulted from microcracks unless sufficient diffusible hydrogen was present and the applied stress exceeded the yield strength of the specimen. Once these facts were recognized, the testing device was redesigned to produce a constant plastic strain during the cracking test. This was done by simply substituting a radiused die block for the four-point bending system as shown schematically in Fig. 1 (right).

The approximate value of the constant plastic, or augmented, strain can be calculated by the relationship:

$$\varepsilon_t = t/2R$$

where ε_t = augmented strain in the outer fibers, t = thickness of the specimen, and R = radius of curvature of the die block (where R >> t).

Therefore, either by substituting a die block with the appropriate radius of curvature, or by changing the thickness of the specimen, any desired augmented strain can be applied to the outer surface of the specimen.

Figure 2 shows a close-up of the device for producing a constant plastic strain with a specimen and a 20 in. (51 cm) radius die block in position. An overall view of the device is shown in Fig. 3. The initiation and propagation of hydrogen induced cracking were documented both by conventional metallography and by microcinematography.

Material

Five heats of HY-80, in the form of 2 in. (51 mm) thick cross-rolled plates in the quenched and tempered condition, were employed in this investigation. The chemical analyses are given in Table 1. The mechanical properties, as determined by the tensile test, were very similar for these five heats, with average values of: 85.0 ksi (586 MPa) yield strength, 106.0 ksi (731 MPa) tensile strength, 26.5% elongation, and 77.7% reduction in area.

Four steels from Heat No. 66U438 (hereafter referred to as Items 1,2,3 and 4) were poured from an open hearth heat having 0.019% S. Mold additions of rare earths amounting to 1, 1¾, and 2½ lb per ton (0.5, 0.88, and 1.25 kg/metric ton) of steel were made to Items 2, 3, and 4, respectively. No additions were made to Item 1, which served as a control. Heat No. 72P305 (from here on referred to as Heat P), another open hearth heat, has a higher C, Ni and Cr content than does Heat No. 66U438. These five heats were selected because of well documented differences in their weldability (Refs. 9, 27, 28).

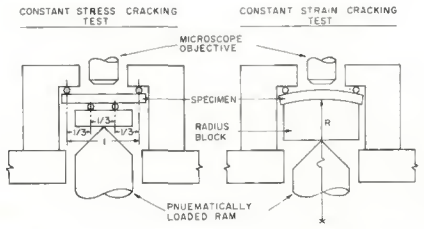

Fig. 1—Schematic illustration of the devices for constant stress cracking test and constant plastic strain cracking test

Fig. 2—Close-up of the device for constant plastic strain cracking test

Specimen Preparation and Testing Procedure

Specimens were cut from 2 in. (51 mm) plates in the manner shown in Fig. 4. Orientation of the banding was transverse to the welding surface, and the location of the bead welds corresponded to the mid-thickness of the plate. The 2 x ½ in. (51 x 13 mm) surfaces were ground parallel and one such surface on each specimen was polished to 6/0 paper. With the polished surfaces of two adjacent specimens in contact, pairs of specimens were welded as shown in Fig. 5. E11018M electrodes, 3/16 in. (4.8 mm) diam, were deposited with an automatic "stick" electrode feeder using 165 A, 22 V and 7.5 ipm (190 mm/min), providing a heat input of approximately 29 kJ/in. (11.4 kJ/cm).

The amount of diffusible hydrogen present in the weldments was controlled by intentionally contaminating the electrode coatings with moisture and then baking at several different temperatures to redry them partially. A 1 x ½ x 1/5 in. (25 x 13 x 5 mm) specimen was welded, as shown in Fig. 5, and the hydrogen content of the weldment was measured by means of the BWRA technique (Ref. 26). The amount of diffusible hydrogen is summarized in Table 2 for the electrode conditioning treatments used in this investigation.

Immediately after welding, the composite weldment was quenched in ice water and then transferred to a bath of dry ice and alcohol (−96 F, −71 C) to minimize the loss of diffusible hydrogen. The specimen to be tested was fractured from the composite weldment and then prepared by standard metallographic techniques to allow direct observation through the microscope. During this preparation, the specimen was cooled frequently in a dry ice-alcohol bath.

In order to study macroscopic crack propagation with the constant elastic stress testing device, several specimens were prepared and tested in the notched condition. After welding, a 1/32 in. (0.8 mm) diam hole was drilled in the center of the weld bead just above the fusion boundary. A saw cut was then made from the surface

of the weld bead to the hole so that the heat-affected zone could be stressed triaxially. To avoid hydrogen loss, the specimens were held in a bath of dry ice and alcohol throughout this notching procedure.

Metallographic Examination and Fracture Study

For metallographic examination, specimens were repolished lightly and etched at about 150 F (66 C) in a 2% aqueous solution of picric acid mixed with a wetting agent. This etchant revealed selectively both the prior austenite grain boundaries and the weld solidification substructures.

Fig. 3—Over-all view of device for constant plastic strain cracking test

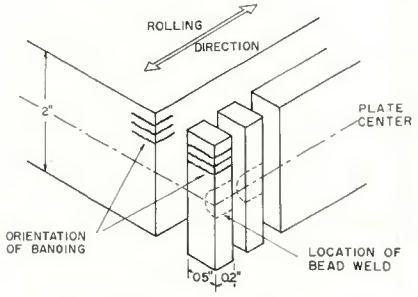

Fig. 4—Orientation of the hydrogen induced cracking test specimens machined from the as-received HY-80 plates

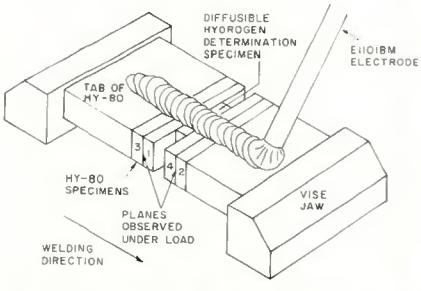

Fig. 5—Schematic illustration showing the welding of specimens

Samples containing hydrogen induced cracking were subsequently fractured at −320 F (−195.8 C). Selected areas of the fracture surface were replicated by a two-stage cellulose acetate-carbon film technique and examined in an electron microscope.

Results and Discussion

Constant Elastic Stress Cracking Tests

As reported by other investigators (Refs. 2,3,15,16), the time to initiate microcracks decreased both as the applied stress increased and as the amount of diffusible hydrogen increased. As shown in Figs. 6 and 7, neither Item 3 nor Heat P experienced hydrogen induced cracking with an estimated diffusible hydrogen content of 8.0 cc/100 g. Note that Heat P exhibited significantly shorter incubation times for crack initiation than did Item 3 and had smaller values of the lower critical stress for crack initiation at the same hydrogen content, as summarized in Table 3. Metallographic examination revealed that the extent of microfissuring in Heat P is more severe than that in Item 3. Thus, Heat P is significantly more sensitive to hydrogen induced cracking than Item 3. It is of interest to note that the cruciform test results (Refs. 9,28) show 7 and 73% cracking for Item 3 and Heat P, respectively. Note that Item 3 contains rare earth elements, while Heat P contains no rare earth elements and is richer than Item 3 in C, Si, Ni, Cr and Mo.

To facilitate the microscopic observation of the evolution of hydrogen, a few drops of immersion oil were spread over the sample surface. It was found that initiation of microcracking was always accompanied by evolution of hydrogen bubbles. This fact was used to determine the incubation time for crack initiation when the cracks were still too small to be detected microscopically. The loading was continued for 24 hrs. and the evolution site was reexamined under a microscope at magnifications up to 750X. In a weld made with an estimated diffusible hydrogen content of 8.0 cc/100 g, evolution of hydrogen bubbles was observed at grain boundaries and nonmetallic inclusions, but no microcracks were observed. Thus, although some

Table 2 — Diffusible Hydrogen Content in the HY-80 Weldments Determined by BWRA Technique

Electrode treatment	Diffusible hydrogen, cc/100 g
Baked at 750 F for 1 h	2.3
Baked at 350 F for 1 h	5.3
Stored in ambient atmosphere	8.1
Fully contaminated by water then baked at 158 F for 20 h	8.0
Fully contaminated by water then baked at 120 F for 20 h	10.5
Fully contaminated by water then baked at 120 F for 1 h	14.1
Fully contaminated by water then baked at 120 F for 15 min	24.0
Fully contaminated by water	32.4

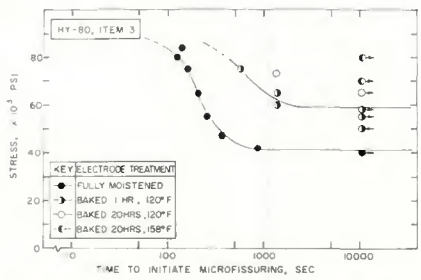

Fig. 6—Applied stress vs time to initiate microfissuring at different hydrogen contents, Item 3. Diffusible H: fully moistened, 32 cc/100 g; baked 1 h, 120 F, 14 cc/100 g; baked 20 h, 120 F, 10.5 cc/100 g; baked 20 h, 158 F, 8 cc/100 g

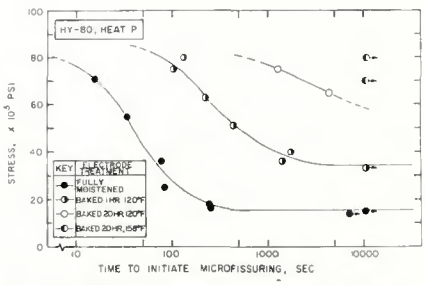

Fig. 7—Applied stress vs time to initiate microfissuring at different hydrogen contents, Item P. Diffusible H: fully moistened, 32 cc/100 g; baked 1 h, 120 F, 14 cc/100 g; baked 20 h, 120 F, 10.5 cc/100 g; baked 20 h, 158 F, 8 cc/100 g

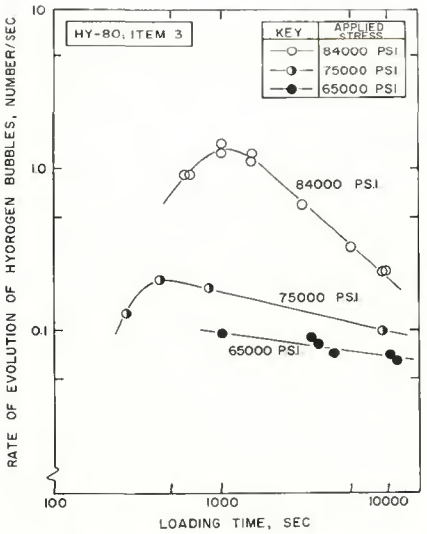

Fig. 8—Rate of evolution of hydrogen bubbles vs loading time, Item 3. Diffusible H: 32 cc/100 g

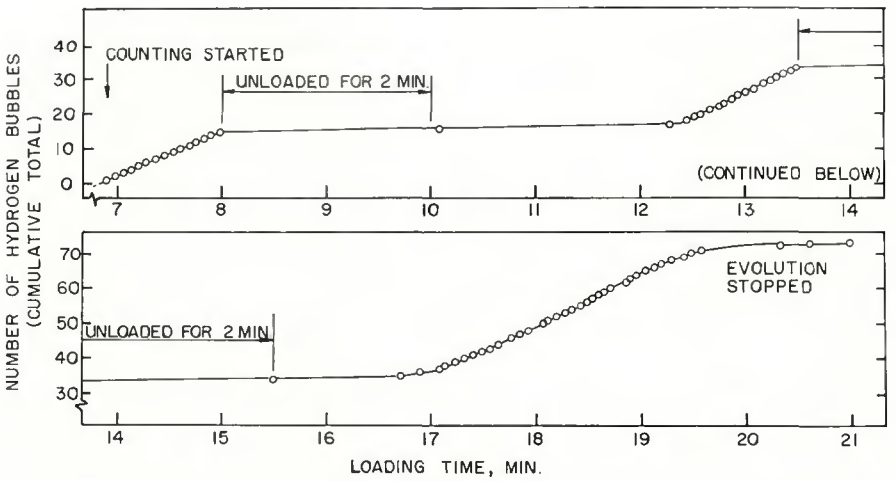

Fig. 9—Result of interrupted loading test. Heat P, 80 ksi applied stress, diffusible H: 32 cc/100 g

Fig. 10—Microcrack initiated from liquated nonmetallic inclusion. Heat P, 16 ksi applied stress, diffusible H: 32/100 g, nital etched. X500, reduced 50%

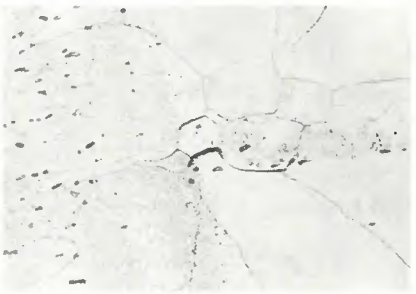

Fig. 11—Microcrack initiated from liquated prior austenite grain boundary. Heat P, 71 ksi applied stress, diffusible H: 32 cc/100 g, (picric acid with wetting agent and nital procedure). X250, reduced 50%

hydrogen was introduced into the weld, the amount was insufficient to cause cracking.

The rate of the evolution of hydrogen bubbles from microscopic cracks was measured during constant elastic stress cracking tests; these results are summarized in Fig. 8. Note that the rate of the evolution of hydrogen bubbles, shown as a function of loading time, increased as applied stress was increased. The rate appeared to increase with time to a maximum characteristic of the particular stress and then decrease with continued exposure to the load.

It appears that increasing the applied stress causes an increase in the rate of diffusion of hydrogen toward the triaxially stressed region ahead of the crack tip. This implies that the diffusion of hydrogen is stress induced.

To examine the stress induced diffusion of hydrogen further, interrupted loading tests were performed. The test data, shown in Fig. 9, were obtained by counting the number of bubbles evolved during three periods of loading and two 2-minute intervals during which the load was removed. Note that the bubble evolution stopped completely immediately after unloading and that upon reloading there was an incubation period before hydrogen evolution was restored. This incubation time can be explained as the time required to develop a critical concentration of hydrogen by stress induced diffusion at the crack tip.

Microscopic cracks were initiated either from previously liquated nonmetallic inclusions or previously liquated grain boundaries, as shown in Figs. 10 and 11, respectively. Liquation was much more evident in Heat P than in Item 3; this can be attributed to the replacement of the complex manganese sulfides (Refs. 8,9) with rare earth sulfides. The rare earth sulfides have higher melting points than complex Mn sulfides and therefore were not liquated in the weld heat-affected zone of Item 3.

None of the constant elastic stress cracking tests performed with stresses below the yield strength of the steel showed macroscopic cracking. However, specimens with a 0.4 mm radius notch with an average stress of 90% of the yield strength, showed extensive macroscopic hydrogen induced cracking. As a microcrack started growing, a significant amount of localized yielding developed in front of the advancing crack tip. Hydrogen evolution accompanied the plastic deformation and the crack continued to grow toward the grain refined region of the heat-affected zone where it was finally arrested. The macroscopic crack growth was "delayed" in nature and the evolution of hydrogen bubbles confirmed the association of hydrogen with the cracking process.

From metallographic examination of subcritical cracks, it appears that thin ellipsoidal sulfide inclusions are very effective as stress raisers and serve as potential crack initiators. Association of elongated sulfides with microcracks was also observed in the unmixed zone near the fusion boundary.

Constant Plastic Strain Cracking Tests

Figure 12 summarizes the results of the constant plastic strain cracking tests on materials from Items 1,2,3, and 4. The total number of cracks observed after 24 hours of loading with an augmented strain of ½% is shown as a function of diffusible hydrogen. It can be seen that Item 3, which contained 1¾ lb/ton (0.87 kg/metric ton) addition of rare earths, is the least sensitive to the cracking and that the control heat, Item 1, which contained no rare earths, is the most sensitive to the cracking. Items 2 and 4 are intermediate in cracking sensitivity. Weldability tests on these materials per-

formed at RPI (Ref. 27) using the Gleeble showed the same trend in their Charpy V-notch toughness. Cruciform test results (Ref. 9) also indicate the large beneficial effect of rare earth additions, but in these tests, Item 4 was rated the least susceptible to the cracking.

Figure 13 demonstrates a comparison of morphology of the nonmetallic inclusions observed in these four steels. It can be clearly seen that as the amount of rare earth elements is increased, the elongated, complex sulfides are replaced by globular rare earth sulfides.

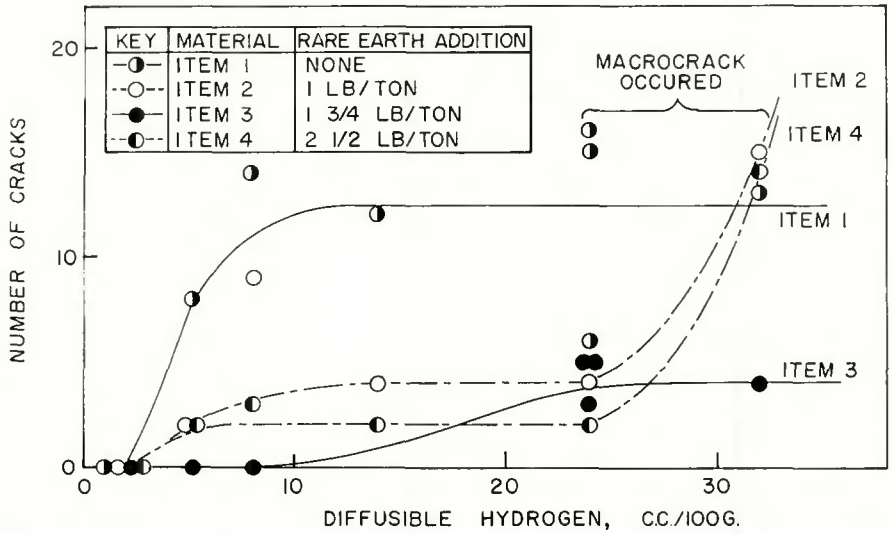

Fig. 12—Total number of cracks vs diffusible hydrogen in the constant strain cracking test. ½% nominal augmented strain

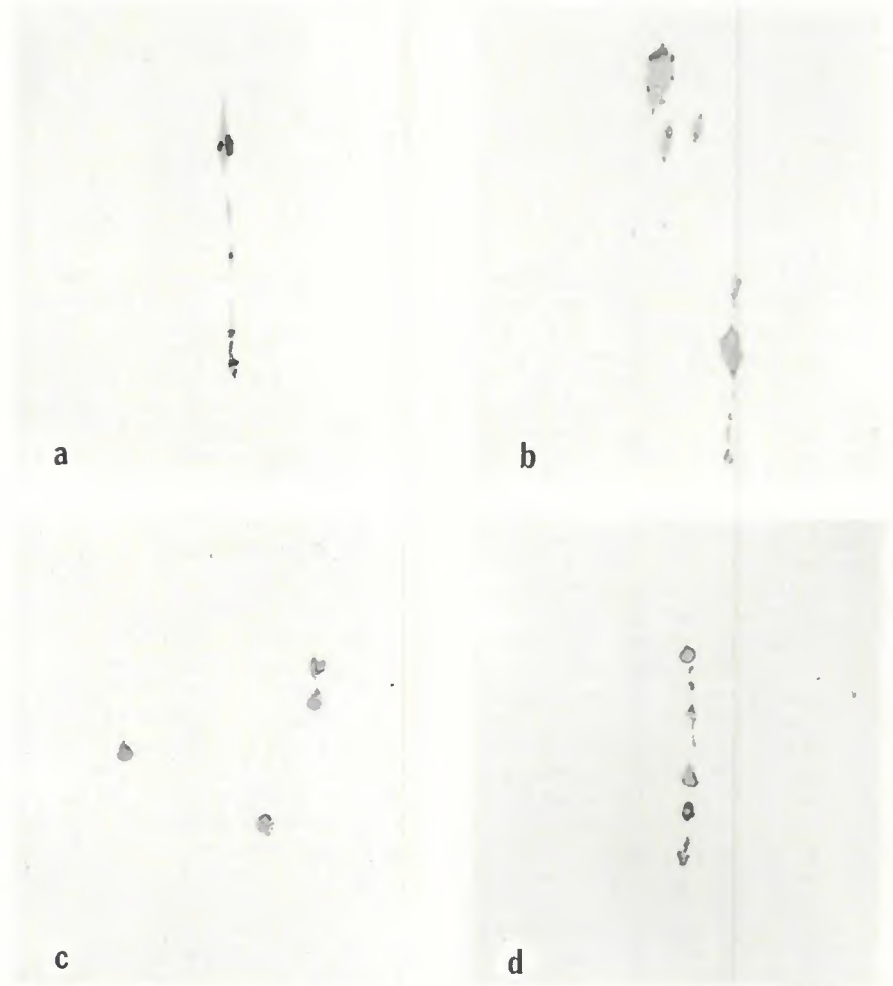

Fig. 13—Photographs of nonmetallic inclusions. Polished and unetched. X500, reduced 28%. (a) Item 1, (b) Item 2, (c) Item 3, (d) Item 4

Figure 14 shows examples of the nucleation of subcritical cracks by the nonmetallic inclusions. Although localized yielding occurred at the tips of the elongated inclusions in Item 1, Fig. 14a, there is no evidence of localized plastic deformation around the globular inclusions in Item 2, Fig. 14b, even though the inclusions themselves have fractured. This suggests that relatively fine globular inclusions formed as a result of the addition of rare earth elements do not cause severe stress concentrations in the surrounding matrix and thus any plastic deformation which does occur is more homogeneous. If sufficient homogeneous plastic deformation occurs in the matrix, the inclusion, being unable to deform plastically, tends to be fractured. This geometric effect and the higher melting point of rare earth sulfides would account for the lower susceptibility of Item 3 to hydrogen induced cracking. A similar beneficial effect of rare earth additions in preventing cold cracking of HY-150 steel weldments has been reported (Ref. 29).

To verify the hypothesis that both plastic strain and hydrogen are necessary to promote macroscopic growth of hydrogen induced cracks, two specimens of Item 4 were welded with conditions which yielded approximately 32 cc/100 g of diffusible hydrogen. One specimen was tested by applying ½% augmented strain for 24 hours immediately after preparing the specimen; the other was tested similarly after having first been degassed in a vacuum for 90 hours at room temperature. In the specimen from which the diffusible hydrogen was removed, no macroscopic crack growth occurred. On the other hand, the hydrogen containing specimen developed an extended macroscopic crack, which initiated from a surface defect in the weld and grew progressively.

To study the development of macrocracks, a series of photomicrographs were taken of the growth process. As an example, Fig. 15 includes sequentially-taken photomicrographs obtained from an Item-1 sample, which was welded under conditions that provided about 32 cc/100 g of diffusible hydrogen and was tested by imposing an augmented strain of ½% for 24 hours. The features of Fig. 15 and the results of a thorough metallographic examination of this sample and a similar one from Item 3 can be summarized as follows:

1. Microcracks are nucleated from either previously liquated, prior austenite grain boundaries or previously liquated, nonmetallic inclusions and/or elongated sulfide inclusions in the heat-affected zone.

2. Before the microcracks start to grow, localized yielding occurs in advance of the crack tip, which is seen as V-shaped roughening of the surface (Refs. 20, 30, 31). The shape of this plastically deformed zone is unstable when the crack is located in the grain coarsened region and becomes relatively more stable as the crack propagates into the grain refined region.

3. The cracking process is both delayed and discontinuous in nature, as has been reported by several investigators (Refs. 2,3,8,16). However, note that the direct observation technique used in this investigation permits a much more vivid description of the propagation kinetics. For example, in Item 1, elongated inclusions provided numerous sharp microcracks in front of the propagating crack and some of these were linked with the main crack as the regions of localized deformation associated with each overlap one another. On the other hand, in Item 3, where the inclusions are rounded, only a few isolated microcracks were formed in advance of the main crack as it propagated.

4. Although under some conditions plastic deformation assists the development of macrocracks as discussed before, it can also inhibit the

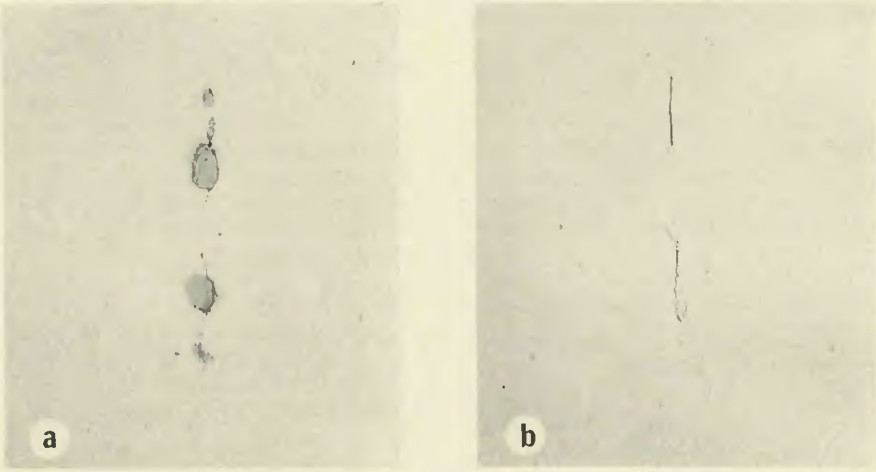

Fig. 14—Subcritical cracks associated with nonmetallic inclusions. Nital etch. X500, reduced 32%. (a) Item 1, (b) Item 2

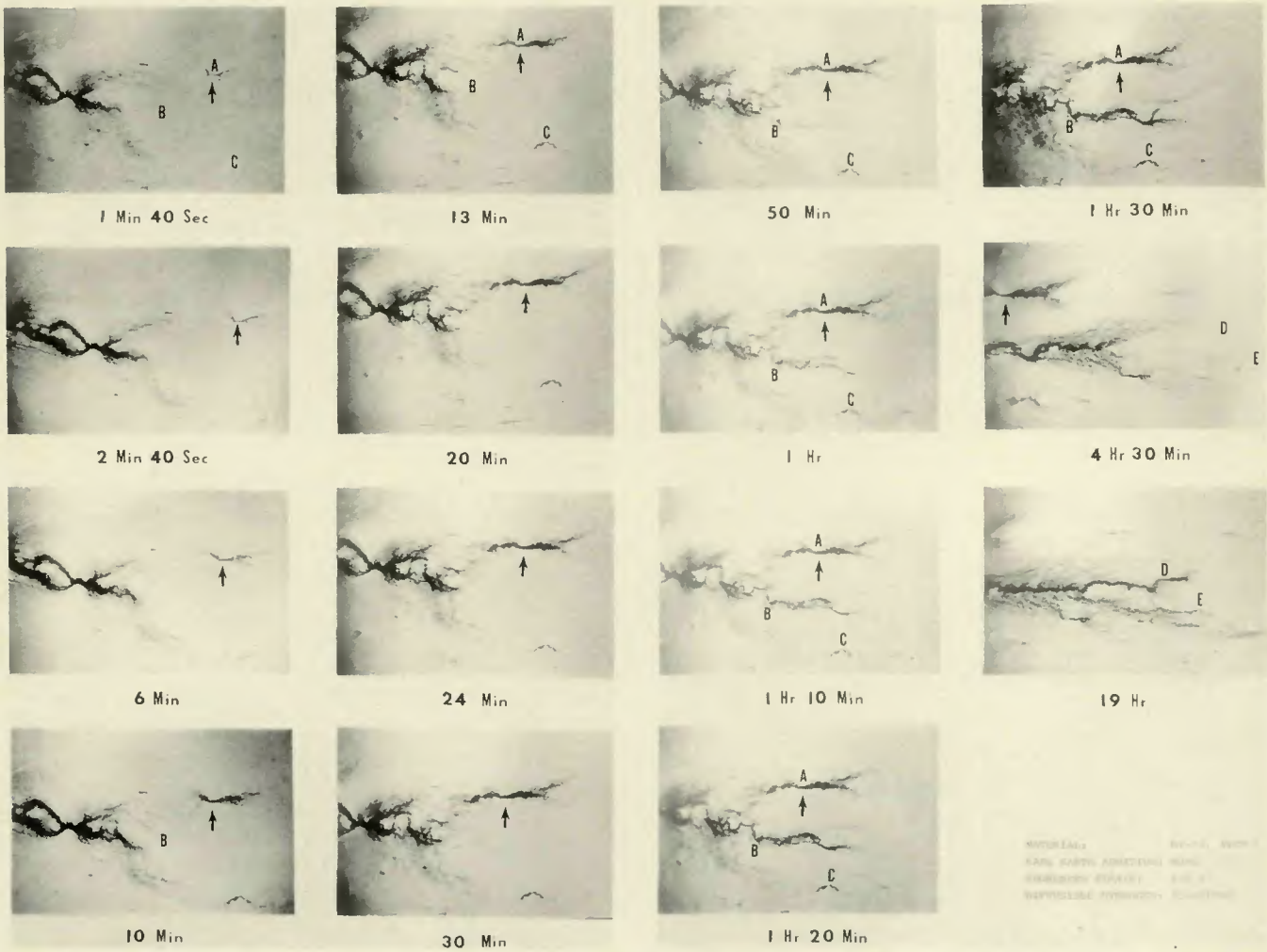

Fig. 15—Hydrogen induced cracking in the constant plastic strain cracking test specimen from Item 1. ½% augmented strain, diffusible H: 32 cc/100 g, nital etch. X60, reduced 43%

development of them. This phenomenon can be seen from the series of photomicrographs in Fig. 15. At 1 min. 40 sec. after straining the specimen exhibits isolated microcracks in front of the main crack at both A and B. As time passes, the growth of crack A is accompanied by greatly increased localized plastic deformation at both ends of the crack. After 24 min. under load, crack A appears to be nearly connected with the main crack while crack B remains as an isolated inactive microcrack. After 50 min. of loading, crack B becomes suddenly active and starts to emit a plastically deformed zone. On the other hand, the tip of crack A is so severely blunted by the plastic deformation that it stops growing. After 4 hrs. and 30 mins. of loading, a macrocrack from crack B still keeps growing and has bypassed crack A completely.

Figures 16 and 17 represent overall views of hydrogen induced cracks in specimens from Items 1 and 3, respectively, tested at 0.8% of augmented strain with a diffusible hydrogen content of 24 cc/100 g. It is clearly evident from these photomicrographs that the plastic deformation is more homogeneous in Item 3 than in Item 1 where the deformation is more localized. It was noted from other tests that both the area experiencing plastic deformation and the width of the main crack increased as the amount of augmented strain increased. However, the total length of the cracks appears to be relatively insensitive to the amount of augmented strain imposed on the specimens.

It was observed that some plastic deformation, and therefore movement of dislocations, occurred locally before microcracks started to grow into macrocracks. Since this localized plastic deformation ahead of a crack tip occurred only when sufficient diffusible hydrogen was present, it must be assumed that the hydrogen which diffuses into the triaxially stressed region ahead of the crack tip helps to make dislocation motion and/or generation easier (Ref. 21).

16 mm motion pictures were taken to document the principal features of crack propagation. These films demonstrate that the V-shaped zone of localized yielding is more extensive as the level of diffusible hydrogen is increased in the weldment. The films also show that the sites of evolution of hydrogen bubbles are usually not located at the tip of a propagating crack but rather are located some distance behind the crack tip.

The evolution of the hydrogen bubbles at some location behind the crack tip can be explained by the Troiano theory of hydrogen embrittlement (Ref. 16). As the crack extends, part of the atomic hydrogen which had diffused into the triaxially-stressed region ahead of the crack tip, will be released because of the reduction of stress concentration. This hydrogen would then diffuse down the newly created crack sur-

Table 3—Summary of Lower Critical Stress for Crack Initiation

Code no.	Diffusible hydrogen, cc/100g	Lower critical stress, ksi
Item 3	32.4	41
Item 3	14.1	59
Heat P	32.4	15
Heat P	14.1	34

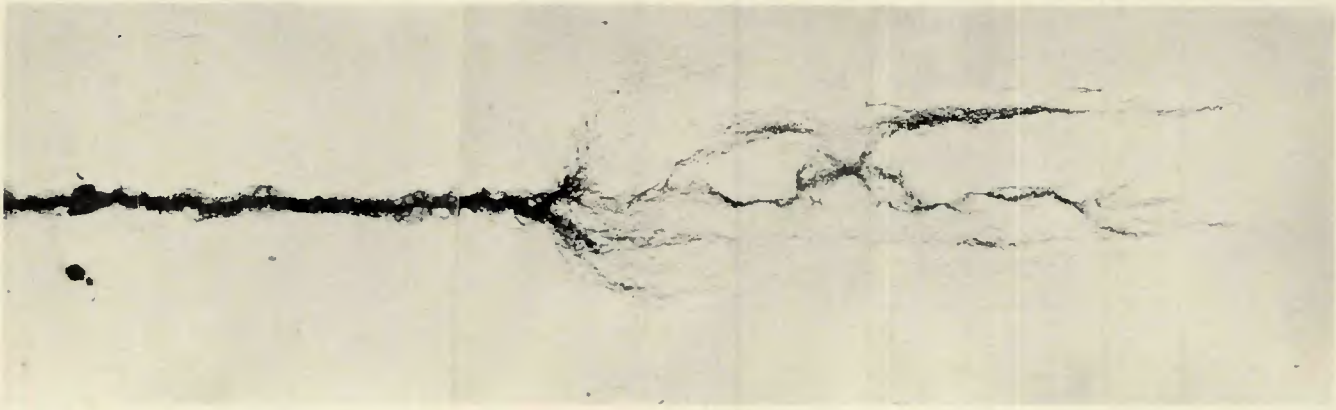

Fig. 16—Overall view of hydrogen induced cracking in Item 1. 0.8% augmented strain for 24 h, diffusible H: 24 cc/100 g, nital etch. X100, reduced 35%

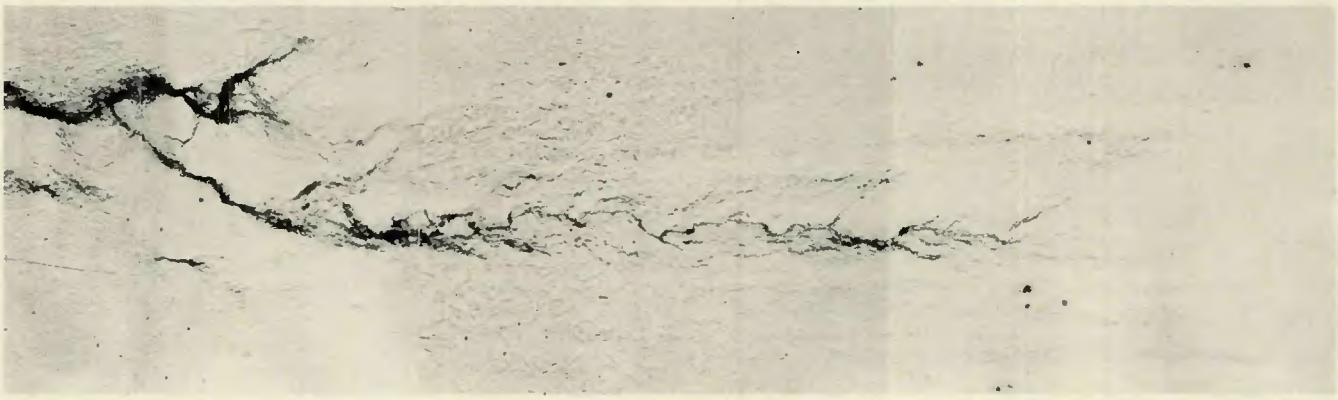

Fig. 17—Overall view of hydrogen induced cracking in Item 3. 0.8% augmented strain for 24 h, diffusible H: 24 cc/100 g, nital etch. X100, reduced 35%

face to appropriate nucleation sites where bubbles of molecular hydrogen would form. Such nucelation sites include, but are not restricted to, the interface between a nonmetallic inclusion and the matrix of a grain boundary which intersects the fractured surface.

Figures 18a and b depict the appearance of typical microcracks in an Item-3 specimen which contained approximately 24 cc/100 g of diffusible hydrogen, and had an augmented strain of 0.8% applied for 24 hours. Note that the cracking is almost exclusively intergranular. On the other hand, the cracking in a similar specimen of Item 1 is mixed intergranular and transgranular in the grain coarsened region, and intergranular in the grain refined region. This variation in cracking morphology can be rationalized by the reasoning summarized below.

The amount of diffusible hydrogen present in the heat-affected zone decreases with increasing distance from the fusion boundary since the weld deposit is the source of hydrogen.

The diffusion of hydrogen occurs more rapidly along grain boundaries and therefore at a given distance from the fusion boundary the hydrogen content of the grain boundaries exceeds that of the adjacent grain matrix.

The transgranular cracking in the coarsened region of the heat-affected zone in Item 1 can be considered to result from the combination of:

1. The high stress intensity at the tips of the elongated inclusions which serve to nucleate microcracks (or microvoids). Thus, the hydrogen diffusion rate is faster, and the hydrogen solubility is higher, in the triaxially stressed region in front of the elongated inclusions in Item 1 than in front of the globular inclusions in Item 3 (Ref. 32).

2. The lowered yield strength at the tip of these elongated inclusions as a consequence of the locally higher solubility for hydrogen. Beachem (Ref. 21) has indicated that hydrogen unlocks dislocations and allows them to multiply or move at reduced stresses.

3. The more localized nature of the plastic deformation in the vincinity of the elongated inclusions, the microcracks, and the tip of the macrocracks. The greater the plastic deformation, and, therefore, the greater the dislocation density, the greater the hydrogen solubility (Ref. 32).

The transition to intergranular cracking in the fine grained region of the heat-affected zone in Item 1 can be explained in terms of the lower level of hydrogen in the matrix at locations this far from the fusion boundary. Thus, the crack propagation shifts to the hydrogen enriched grain boundaries at some critical distance from the fusion boundary.

The almost exclusively intergranular fracture observed in Item 3 reflects the lower stress intensity associated with the globular inclusions. This in turn requires the facture path to seek out the hydrogen enriched grain boundaries even in the grain coarsened region because the hydrogen content of the matrix is insufficient to sustain quasi-cleavage fracture at this lower stress-intensity factor.

The majority of the fracture surfaces in the heat-affected zone exhibited an intergranular fracture mode, as was discussed above in connection with the conventional metallographic study. Figure 19 is an electron micrograph taken at 5500X of a replica of a crack in a specimen of Item 3. This fractograph shows the typical appearance of the intergranular-type fracture observed in this specimen.

Conclusions

The conclusions drawn from this investigation are:

1. The augmented-strain cracking test procedure has been shown to be an excellent method to produce hydrogen induced cracking in laboratory scale specimens.

2. The test results indicate that this procedure allows quantitative rating of the susceptibility of steels to hydrogen induced cracking.

3. Among the four lots of HY-80 steel examined, the results indicate that:

a. Item 3, which contained a ladle addition of 1¾ lb/ton of rare earth elements, is the least sensitive to hydrogen induced cracking.

b. Item 1, which contained no rare earth addition, is the most sensitive to hydrogen induced cracking.

c. The crack sensitivity of both Item 2 and Item 4, which contained rare earth additions of 1 and 2½ lb/ton, respectively, are intermediate between that of Item 1 and that of Item 3, with Item 2 being slightly inferior to Item 4.

4. The results of the direct observation of the nucleation and propagation of hydrogen induced cracking indicate that:

a. A certain amount of microscopic yielding must occur locally before microcracks start to grow.

b. Hydrogen is necessary for the propagation of cracks and appears to make the localized deformation process easier.

c. Hydrogen induced cracking can be nucleated by previously liquated grain boundaries and/or liquated nonmetallic inclusions in the unmixed zone and partially melted zone.

d. In the true heat-affected zone, hydrogen induced cracking can be nucleated by elongated sulfide inclusions.

e. The planar-pressure mechanism appears to play no part in the propagation of cracks.

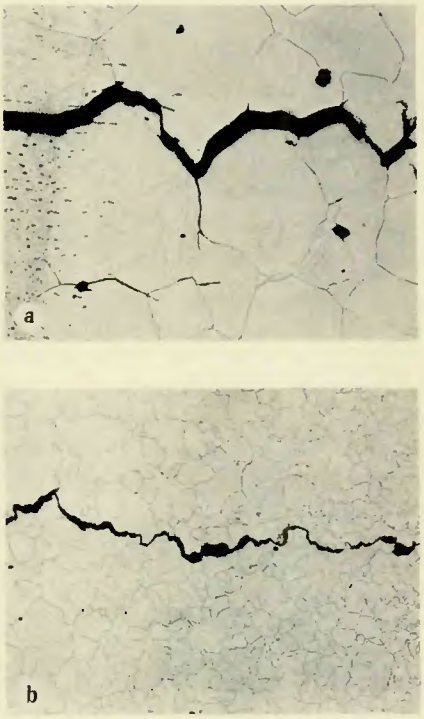

Fig. 18—Hydrogen induced cracking produced in 24 h with 0.8% augmented strain. Diffusible H: 24 cc/100 g. 2% picric acid and wetting agent etch. X250, reduced 50%

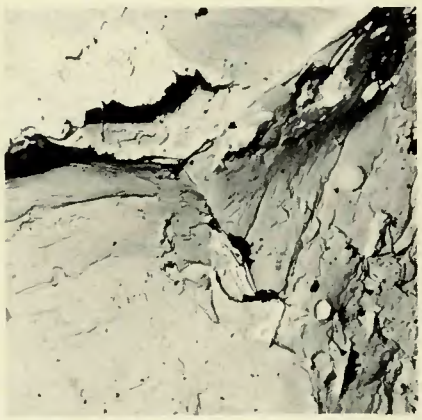

Fig. 19—Electron micrograph of the fracture surface of a specimen strained at ½% augmented strain. X5,500, reduced 28%

References

1. Baker, R. G., "Weld Cracking — A Modern Insight," *Brit. Weld. J., 15* (6), 283-295 (1968).

2. Boniszewski, T., Watkinson, F.,

Baker, R. G., and Tremlett, H. F., "Hydrogen Embrittlement and Heat-Affected Zone Cracking in Low-Carbon Alloy Steels with Acicular Microstructures," *Brit. Weld. J., 12* (1) 14-36 (1965).

3. Boniszewski, T., and Baker, R. G., "Hydrogen Embrittlement in Low Carbon Nickel and Manganese Steels," *Brit. Weld. J.,* 12 (7), 349-362 (1965).

4. Graville, B. A., "Effect of Hydrogen Concentration on Hydrogen Embrittlement," *Brit. Weld. J.,* 15 (4), 191-195 (1968).

5. Interrante, C. G., and Stout, R. D., "Delayed Cracking in Steel Weldments," *Welding J.,* 43 (4), April 1964, Research Suppl., 145-s to 160-s.

6. Evans, G. M., and Christensen, N., "Correlation of Weld Metal Hydrogen Content with HAZ Embrittlement," *Metal Construct.* and *Brit. Weld. J., 3* (5), 188-189 (1971).

7. Savage, W. F., and Szekeres, E. S., "A Mechanism for Crack Formation in HY-80 Steel Weldments," *Welding J.,* 46 (2), Feb. 1967, Research Suppl., 94-s to 96-s.

8. Savage, W. F., Nippes, E. F., and Szekeres, E. S., "A Study of Hydrogen-Induced Cold Cracking in a Low-Alloy Steel," *Welding J.,* 55 (9), Sept. 1976, Research Suppl, 276-s to 283-s.

9. Wilson, W. G., "Reduced Heat-Affected Zone Cracking and Improved Base Metal Impacts Through Sulfide Control with Rare Earth Additions," *Welding J.,* 50 (1), Jan. 1971, Research Suppl., 42-s to 46-s.

10. Bernstein, I. M., "The Role of Hydrogen in the Embrittlement of Iron and Steel," *Materials Science Eng., 6* (1), 1-19 (1970).

11. Zapffe, C. A., and Sims, C. E., "Hydrogen Embrittlement, Internal Stress and Defects in Steel," *Trans. AIME, 145,* 225-261 (1941).

12. Tetleman, A. S., Fracture of Solids, John Wiley and Sons, New York, (1962).

13. Petch, N. J., "The Lowering of Fracture-Stress Due to Surface Adsorption," *Phil. Mag.,* 1, 331-337 (1956).

14. Williams, D. P., and Nelson, H. G., "Embrittlement of 4130 Steel by Low-Pressure Gaseous Hydrogen," *Metallurgical Trans.,* 1 (1), 63-68 (1970).

15. Barth, C. F., and Steigerwald, E. A., "Evaluation of Hydrogen Embrittlement Mechanisms," *Metallurgical Trans.,* 1 (12), 3451-3455 (1970).

16. Troiano, A. R., "The Role of Hydrogen and Other Interstitials on the Mechanical Behavior of Metals," *Trans. ASM,* 52 (1), 54-80 (1960).

17. Frohmberg, R. P., Barnett, W. J., and Troiano, A. R., "Delayed Failure and Hydrogen Embrittlement in Steel," *Trans. ASM,* 47, 892-925 (1955).

18. Rogers, H. C., "The Influence of Hydrogen on the Yield Point in Iron," *Acta Met.,* 4 (3), 114-117 (1956).

19. de Kazinczy, F., "Effect of Hydrogen on the Yielding of Mild Steel," *Acta Met.,* 7 (11), 706-708 (1959).

20. Vennett, R. M., and Ansell, G. S., "The Effect of High-Pressure Hydrogen Upon the Tensile Properties and Fracture Behavior of 304L Stainless Steel," *Trans. ASM,* 60 (2), 242-251 (1967).

21. Beachem, C. D., "A New Model for Hydrogen-Assisted Cracking (Hydrogen Embrittlement)," *Metallurgical Trans.,* 3 (2), 437-451 (1972).

22. Steinman, J. B., Van Ness, H. C., and Ansell, G. S., "The Effect of High-Pressure Hydrogen Upon the Notch Tensile Strength and Fracture Mode of 4140 Steel," *Welding J.,* 44 (5), May 1965, Research Suppl., 221-s to 224-s.

23. Steigerwald, E. A., Schaller, F. W., and Troianao, A. R., "Discontinuous Crack Growth in Hydrogenated Steel," *Trans. AIME,* 215 (12), 1048-1052 (1959).

24. Hartbower, C. E., Gerberich, W. W., and Crimmons, P. P., "Monitoring Subcritical Crack Growth by Detection of Elastic Waves," *Welding J.,* 47 (1), Jan. 1968, Research Suppl., 1-s to 18-s.

25. Granjon, H. P., "Studies on Cracking of and Transformation in Steels During Welding," *Welding J.,* 41 (1), Jan. 1962, Research Suppl., 1-s to 11-s.

26. Coe, F. R., "Hydrogen in Weld Metal," Brit. Weld. Research Association Bulletin, 8 (3), 76-81 (1967).

27. Ledman, J. L., Lundin, C. D., and Savage, W. F., "Study of the Transformational Characteristics and the Weldability of HY-80 Steel," Rensselaer Polytechnic Institute Final Report, Contract 78813, Jan. (1963).

28. Rathbone, A. M., and Gross, J. H., "Factors Influencing Heat-Affected Zone Cracking of HY-80 Steel Weldments," Technical Report 56.02-001 (4), U.S. Steel Corp., Applied Res. Lab., Monroeville, Pa., June (1962).

29. Meitzner, C. F., and Stout, R. D., "Microcracking and Delayed Cracking in Welded Quenched and Tempered Steel," *Welding J.,* 45 (9), Sept. 1966, Research Suppl., 393-s to 400-s.

30. Baillie, J. G., "Underbead and Toe Cracks," *Brit. Weld. J.,* 14 (2), 51-61 (1967).

31. Venett, R. M., and Ansell, G. S., "A Study of Gaseous Hydrogen Damage in Certain FCC Materials," Trans. ASM, 62 (4), 1007-1012 (1969).

32. Bockris, J. O'M., Beck, W., Grenshaw, M. A., Subramanyan, P. K. and Williams, F. S., "The Effect of Stress on the Chemical Potential of Hydrogen," *Acta Met.,* 19 (11), 1209-1218 (1971).